

# Re–Os dating of molybdenite and in-situ Pb isotopes of sulfides from the Lamo Zn–Cu deposit in the Dachang tin-polymetallic ore field, Guangxi, China

Hai Zhao<sup>1,2</sup> · Wenchao Su<sup>1,6</sup> · Peng Xie<sup>1,2</sup> · Nengping Shen<sup>1</sup> · Jiali Cai<sup>1</sup> · Ming Luo<sup>3</sup> · Jie Li<sup>4</sup> · Zhian Bao<sup>5</sup>

Received: 3 October 2017 / Revised: 11 January 2018 / Accepted: 7 February 2018 / Published online: 15 February 2018  
© Science Press, Institute of Geochemistry, CAS and Springer-Verlag GmbH Germany, part of Springer Nature 2018

**Abstract** The Dachang tin-polymetallic district, Guangxi, China, is one of the largest tin ore fields in the world. Both cassiterite-sulfide and Zn–Cu skarn mineralization are hosted in the Mid-Upper Devonian carbonate-rich sediments adjacent to the underlying Cretaceous Longxianggai granite (91–97 Ma). The Lamo Zn–Cu deposit is a typical skarn deposit in the district and occurs at the contact zone between the Upper Devonian limestone and the granite. The ore minerals mainly consist of sphalerite, arsenopyrite, pyrrhotite, galena, chalcopyrite, and minor molybdenite. However, the age of mineralization and source of the metals are not well constrained. In this study, we use the molybdenite Re–Os dating method and in-situ Pb isotopes of sulfides from the Lamo deposit for the first time in order to directly determine the age of mineralization and the tracing source of metals. Six molybdenite samples yielded a more accurate Re–Os isochron age of  $90.0 \pm 1.1$  Ma

(MSWD = 0.72), which is much younger than the reported garnet Sm–Nd isochron age of  $95 \pm 11$  Ma and quartz fluid inclusions Rb–Sr isochron age of  $99 \pm 6$  Ma. This age is also interpreted as the age of Zn–Cu skarn mineralization in the Dachang district. Further, in this study we found that in-situ Pb isotopes of sulfides from the Lamo deposit and feldspars in the district's biotite granite and granitic porphyry dikes have a narrow range and an overlap of Pb isotopic compositions ( $^{206}\text{Pb}/^{204}\text{Pb} = 18.417\text{--}18.594$ ,  $^{207}\text{Pb}/^{204}\text{Pb} = 15.641\text{--}15.746$ , and  $^{208}\text{Pb}/^{204}\text{Pb} = 38.791\text{--}39.073$ ), suggesting that the metals were mainly sourced from Cretaceous granitic magma.

**Keywords** Molybdenite Re–Os dating · In-situ lead isotopes · Skarn deposit · Dachang

## 1 Introduction

The Dachang tin-polymetallic district, Guangxi, China, is one of the largest tin ore fields in the world and contains approximately 1.5 Mt Sn, 6.8 Mt Zn, 1.8 Mt Pb, 1.4 Mt Sb, 0.4 Mt Cu, and other metals (Huang et al. 2012). Economic deposits in the district include the Lamo proximal skarn Zn–Cu deposit, the Tongkeng-Changpo and Gaofeng tin-base metal deposits, and the Huile and Dafulou black shale-hosted cassiterite-sulfide deposits. They occur as stratiforms, veins, and stockworks that are hosted in the Mid-Upper Devonian carbonate-rich sediments adjacent to the underlying Cretaceous Longxianggai granite.

In the past decades, there were a large number of studies on the geology, mineralogy, geochemistry, isotopes, chronology, and fluid inclusions for the Dachang ore district (Chen et al. 1985, 1993; Han and Hutchinson 1989a, b; Fu et al. 1991, 1993; Zhao et al. 2002, 2007; Pašava et al.

✉ Wenchao Su  
suwenchao@vip.gyig.ac.cn

<sup>1</sup> State Key Laboratory of Ore Deposit Geochemistry, Institute of Geochemistry, Chinese Academy of Sciences, Guiyang 550081, China

<sup>2</sup> University of Chinese Academy of Sciences, Beijing 100049, China

<sup>3</sup> Limited Company of Jilang Indium Industries, Nandan 547200, China

<sup>4</sup> State Key Laboratory of Isotope Geochemistry, Guangzhou Institute of Geochemistry, Chinese Academy of Sciences, Guangzhou 510640, China

<sup>5</sup> State Key Laboratory of Continental Dynamics, Department of Geology, Northwest University, Xi'an 710069, China

<sup>6</sup> Present Address: 99 Linchengxi Road, Guanshanhu District, Guiyang 550081, China

2003; Cai et al. 2004, 2005, 2006a, b; Fan et al. 2004; Wang et al. 2004, 2015; Li et al. 2008; Liang et al. 2011a, b; Xu et al. 2011), but the origin of the deposits remains controversial. Most studies concluded that all of deposits in the Dachang district were formed in a magmatic hydrothermal system related to the Longxianggai granite (Chen et al. 1993; Fu et al. 1991, 1993; Cai et al. 2005, 2007; Li et al. 2008), based on similar age ranges for mineralization (91–96 Ma) and for the granite (91–97 Ma) (Wang et al. 2004, 2015; Cai et al. 2006a, b, 2011a, b; Guo et al. 2017). Others argued that some ores, especially the stratiform ores, were the results of submarine exhalations during the Devonian (Cai and Zhang 1983; Han and Hutchinson 1989a, b, 1997; Jiang et al. 1999; Zhao et al. 2007). These debates may be attributed to the lack of convincing chronological data, especially the lack of direct dating on sulfides, as this data were determined by different isotopic dating methods.

Re–Os isotope system is widely used for direct dating of sulfides for the deposits because some sulfides contain detectable Re and Os concentrations. Many studies have shown that molybdenite ( $\text{MoS}_2$ ) is the most suitable sulfide for the direct dating of mineralization, owing to its high concentration of Re (up to hundreds or thousands of parts per million) but lack of common Os (Luck and Allegre 1982; Selby and Creaser 2001; Stein et al. 2001). Recent mining reveals that molybdenite occurs locally in the skarns associated with Zn–Cu mineralization at the Lamo deposit in the Dachang ore field. This provides a good opportunity to directly date Zn–Cu mineralization. In this paper, we are the first to report a precise age for Zn–Cu mineralization in the Dachang district, using the molybdenite Re–Os dating method. Combined with in-situ Pb isotope of sulfides from the Lamo deposit and feldspars in the biotite granite and granitic porphyry dikes in the district, the sources of metals for the Lamo deposit are also discussed.

## 2 Geological setting

The Dachang tin-polymetallic ore field (Fig. 1) is located in the central part of the Danchi fold belt, at the intersection between the Jiangnan geoanticline and the Tiengui geosyncline (Cai et al. 2007). Sedimentary rocks in this area consist of Devonian siltstone, black shale, lenticular and reef limestone, Carboniferous limestone and siltstone, and Permian sandstone. These rocks are exposed along the axis of the NW-trending Longxianggai anticline and are cut by the Longxianggai reverse fault on the west flank, where the Longxianggai granite intruded. A series of the NE-trending normal faults cut the anticline and the reverse fault. In addition, there is a small anticline that developed

in the southwestern part of the district. The axis of the Dachang anticline is parallel to the main fold and is cut by the Dachang reverse fault, where the granite porphyry dikes intruded.

The Longxianggai granite is the main intrusive body in the Dachang area. It crops out at the center part of the Dachang ore field, with an area of  $0.5 \text{ km}^2$ , near the axis of the Longxianggai anticline (Fig. 1). It contains quartz (36%), K-feldspar (38%), plagioclase (22%), muscovite (3%), and biotite (1%), with accessory ilmenite, zircon and monazite (Fu et al. 1991). The granite and its porphyritic phase have been dated by the SHRIMP zircon U–Pb dating at  $93 \pm 1$  and  $91 \pm 1$  Ma, respectively (Cai et al. 2006a). However, Liang et al. (2011a, b) reported slightly older ages for the granite, ranging from  $94 \pm 1$  to  $97 \pm 3$  Ma, and these ages were measured by the LA-MC-ICP-MS zircon U–Pb dating method.

Mineralization in the Dachang ore field exhibits obvious metal zoning, both vertical and horizontal, around the Longxianggai granite pluton. The Lamo Zn–Cu skarn deposit occurs in the contact areas between the Upper Devonian limestone and the granite, whereas the cassiterite-sulfide ores are mainly distributed distal to the granite, such as the Changpo-Tongkeng and Gaofeng deposits in the western part, and the Dafulou, Huile and Kangma deposits in the eastern part.

## 3 Geology of deposit

The Lamo Zn–Cu deposit (Fig. 2) is a typical skarn deposit in the Dachang ore field and has many characteristics of proximal calcic skarns (Kwak 1987). It contains approximately 0.6 Mt Zn with an average grade of 4% Zn, 0.034 Mt Cu with an average grade of 0.6% Cu, and other metals (Ye and Pan 1994). The geology of the deposit was described in detail by Fu et al. (1991).

Sedimentary rocks in the Lamo district consist of marl and shale of the Middle Devonian Luofu Formation, siliceous rocks of the Upper Devonian Liujiang Formation, lenticular and banded limestone of the Upper Devonian Wuzhishan Formation, and marl, mudstone and shale of the Lower Carboniferous Luzhai Formation. Zn–Cu ores are hosted in the contact zone between the lenticular and banded limestone of the Upper Devonian Wuzhishan Formation and the granite. The limestone within 1–1.5 km of the granite contact had been metamorphosed to marble, hornfels, and metamorphic skarns (Fu et al. 1991).

The orebodies at the Lamo occur as chimney, mantos, and pods (Fu et al. 1991). Ore minerals mainly consist of sphalerite, arsenopyrite, pyrrhotite, galena, chalcopyrite, and minor molybdenite and scheelite. Based on field observation, crosscutting relations and mineral

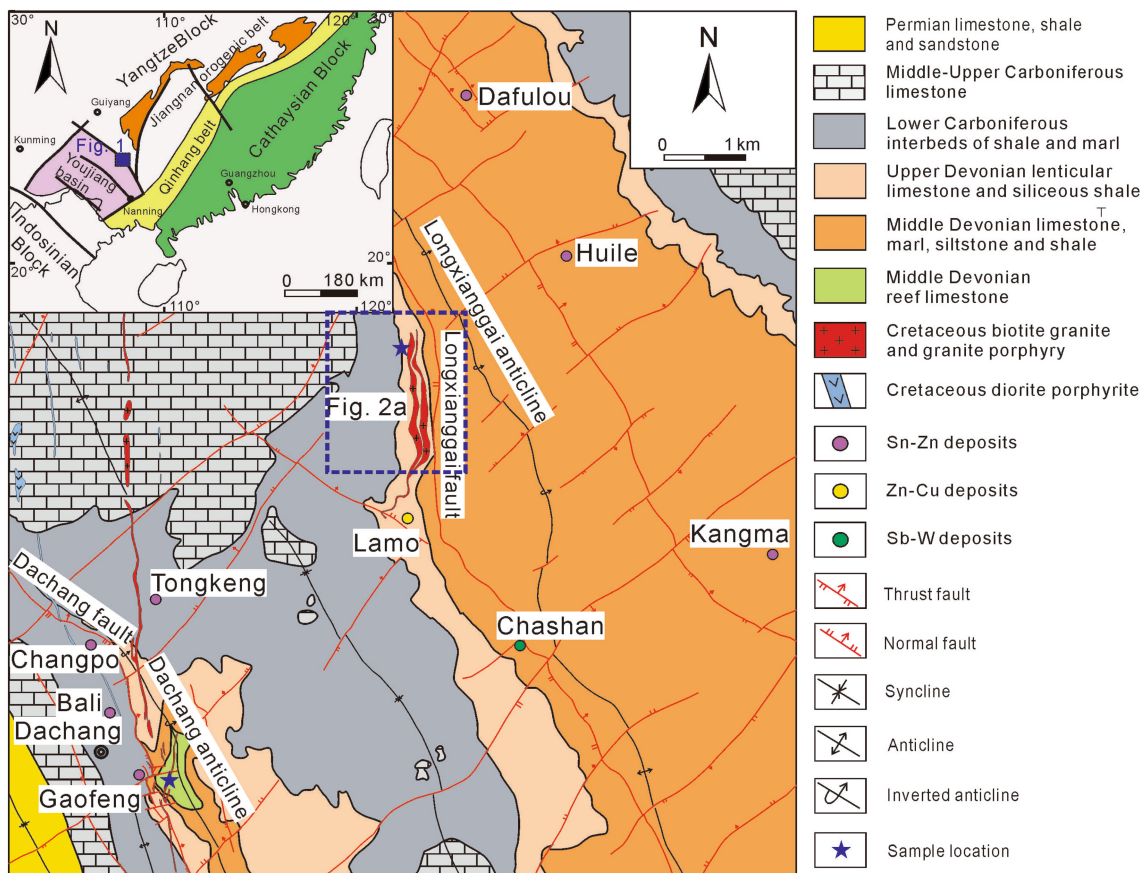


**Fig. 1** Geological map of the Dachang ore field (modified from Chen et al. 1993)

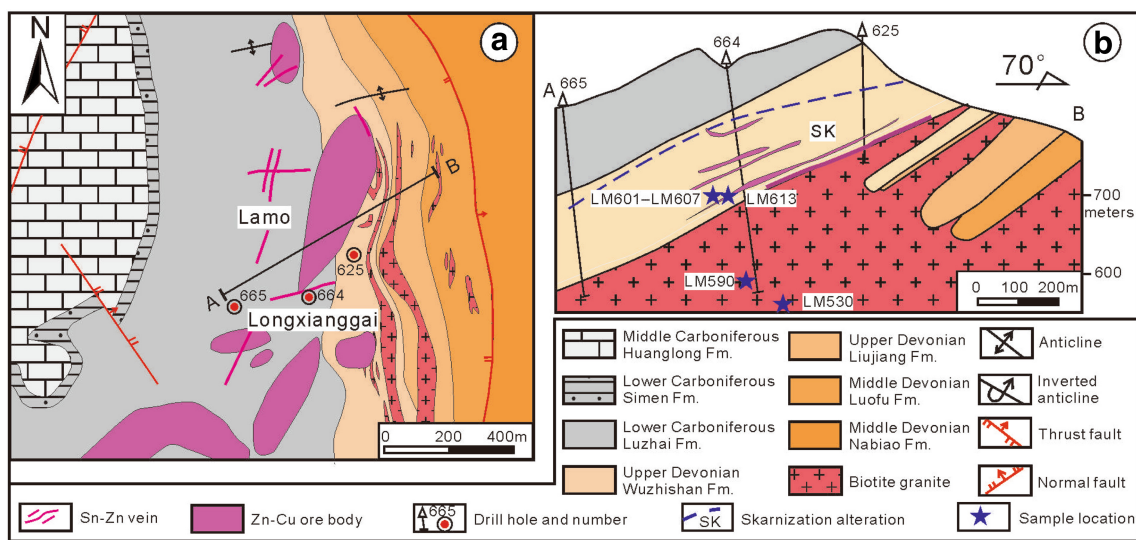


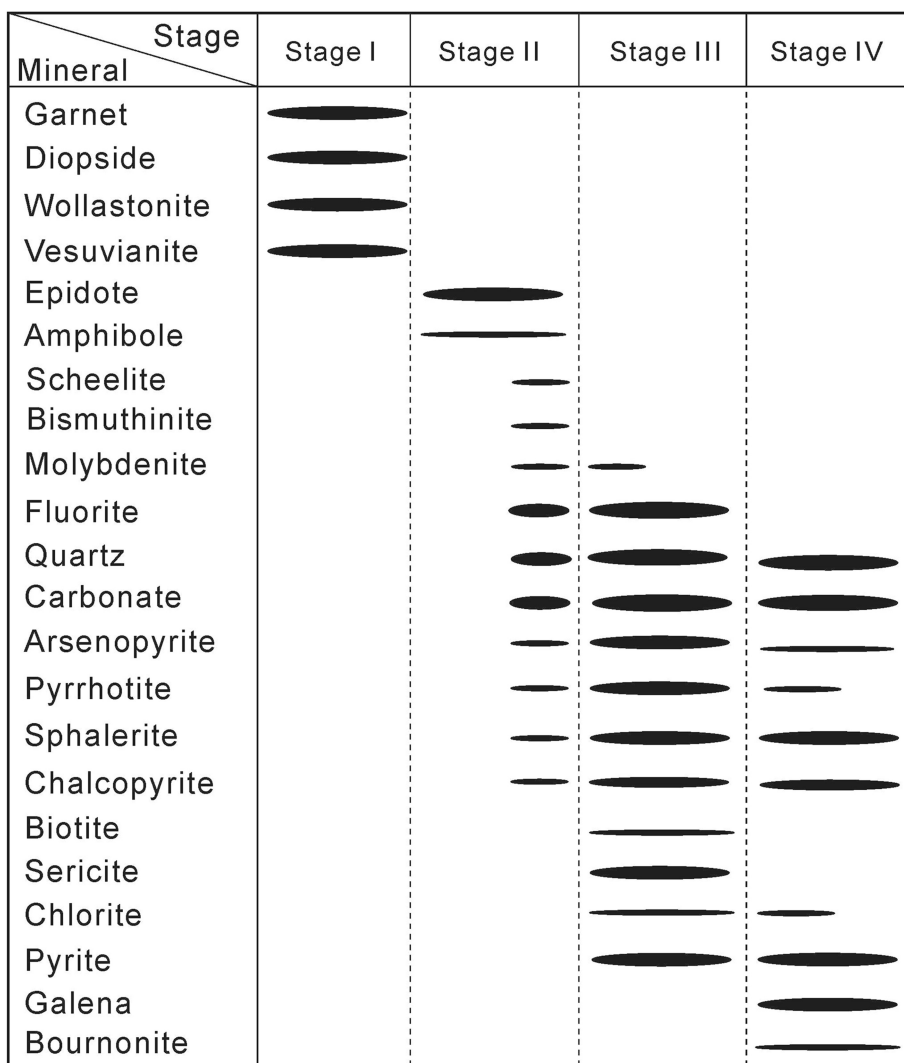
**Fig. 2** Geological map (a) and cross-section map (b) of the Lamo Zn-Cu deposit (modified from Chen et al. 1993)

assemblages, four mineral stages for the Lamo deposit have been identified (Fig. 3).

Stage I and II are skarn assemblages, which occur only near the granite contact. Stage I is a dry skarn stage and consists of garnet, vesuvianite, and wollastonite, with

minor diopside. The garnet is usually light brown in color (Fig. 4a–e) and composed 60% to 70% grossular and 30% to 40% andradite (Fu et al. 1991, 1993). Vesuvianite is typically subhedral and intergrown with garnet and wollastonite. Fluid inclusion studies indicated that this stage

**Fig. 3** Paragenetic sequence of minerals for the Lamo Zn–Cu deposit



has high homogenization temperature from 582 to 645 °C, with salinities of 7 wt%–9 wt% NaCl equiv (Fu et al. 1993).

Stage II is a wet skarn stage and contains epidote, amphibole, fluorite, and quartz. These minerals commonly replaced the garnet, diopside, and vesuvianite of the Stage I. Sulfide mineralization began to develop in this stage and occur as stratiform (Fig. 4d, e) or be disseminated in the skarns (Fig. 4b). Sulfide minerals include sphalerite, arsenopyrite, pyrrhotite, minor molybdenite, bismuthinite and chalcopyrite, which fill or replace the garnet and diopside (Fig. 4c, f). Fluid inclusion studies showed that this stage was formed at temperatures from 359 to 396 °C, with salinities of 13 wt%–47 wt% NaCl equiv (Fu et al. 1993).

Stages III and IV are considered the ore sulfide stages that occur as massive ores (Fig. 4g) in the outermost zone adjacent to marble. Stage III contains various sulfides and hydroxyl-bearing silicates, including biotite, sericite,

chlorite, sphalerite, arsenopyrite, galena, pyrite, pyrrhotite, and minor chalcopyrite (Fig. 4h). Stage IV is dominated by quartz, carbonates, chlorite, sphalerite, galena, pyrite, minor chalcopyrite and bournonite.

#### 4 Sampling and analytical methods

The ten samples analyzed in this study were collected from the Lamo deposit and the Dachang ore field. Seven samples were collected from the underground tunnels (680 m level) at the Shamuchong part of the Lamo deposit (Fig. 2). They occurred within the skarn zones close to the granite. Re–Os dating samples (LM-601, LM-603, LM-604, LM-605, LM-606, and LM-607) were collected from the same molybdenite veinlet (Fig. 4a). They contain garnet, diopside, molybdenite, minor bismuthinite and scheelite (Fig. 4b, c). One ore sample (LM613) selected for in-situ Pb isotopes analyses was from the same skarn zone that hosted the

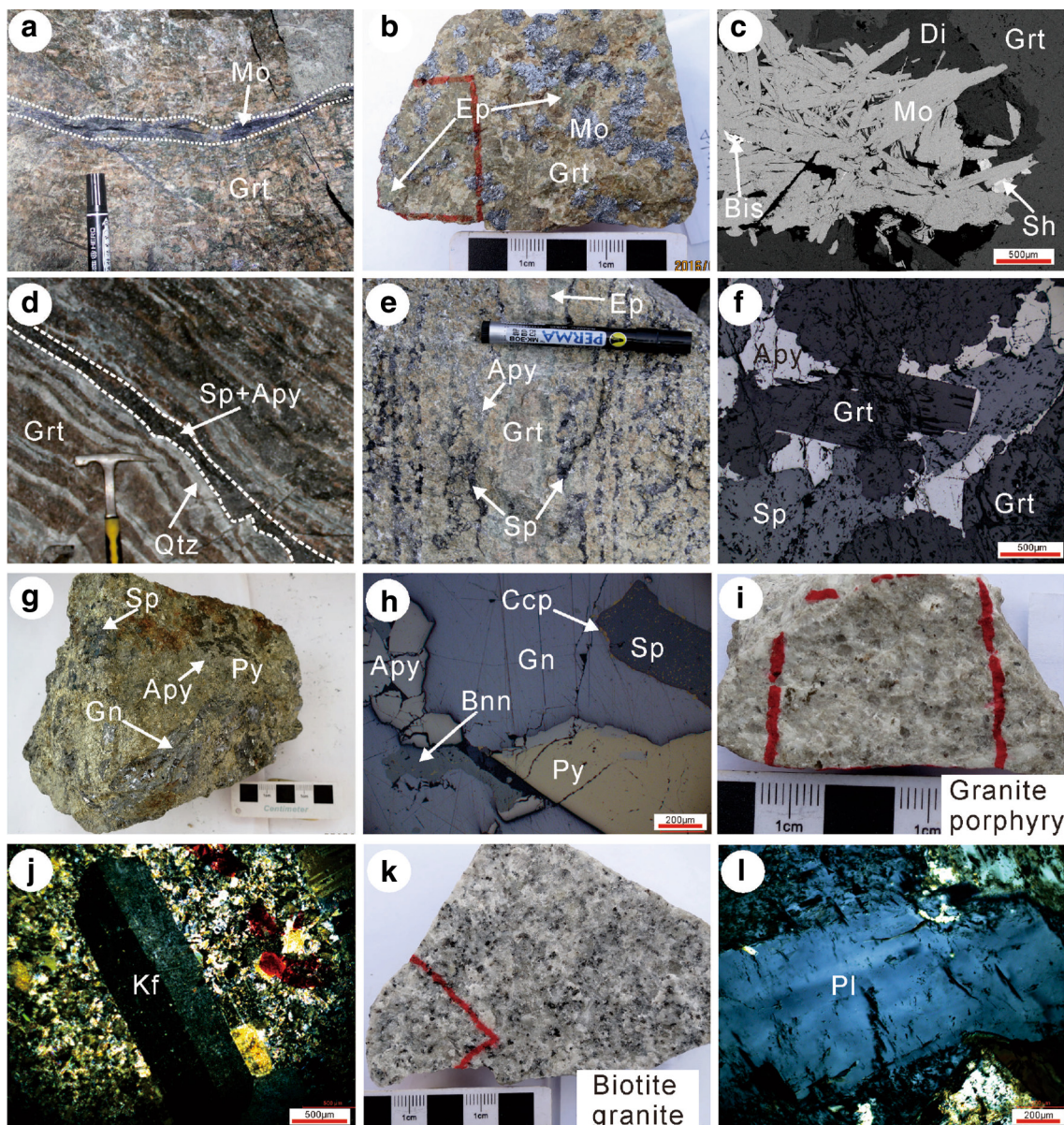


**Fig. 4** Examples of ores from the Lamo deposit and feldspars of the granite in the Dachang ore field. **a** Molybdenite occurs as veinlets in skarn. **b** A hand specimen showing disseminated molybdenite associated with garnet and epidote. **c** SEM back-scattered electron (BSE) image showing molybdenite intergrown with scheelite, bismuthinite, diopside and garnet. **d, e** Stratiform sulfide ore containing sphalerite and arsenopyrite occurred in the skarn. **f** Arsenopyrite and sphalerite fill or replaced garnet (BSE). **g** Massive sulfide ores in the Lamo deposit. **h** Pyrite, arsenopyrite, and sphalerite in the massive ores replaced by galena and bournonite. **i** Granite porphyry and its K-feldspar **j** from the Gaofeng tin-polymetallic ore deposit. **k** Biotite granite and its plagioclase **l** from the Longxianggai pluton. *Kf* K-feldspar; *Pl* plagioclase; *Mo* molybdenite; *Grt* garnet; *Ep* epidote; *Di* diopside; *Py* pyrite; *Apy* arsenopyrite; *Sp* sphalerite; *Ccp* chalcopyrite; *Bis* bismuthinite; *Sh* scheelite; *Bnn* bournonite; *Gn* galena

molybdenite veinlet at the Lamo deposit (Fig. 2b). It is dominated by sphalerite, arsenopyrite, galena, pyrite, minor chalcopyrite and bournonite (Fig. 4g, h). To compare with the Pb isotopes of sulfides, two granite samples (LM530 and LM590) were collected from the 530 m and 590 m level of tunnels at the Lamo deposit (Fig. 2), respectively. One granite porphyry sample (GF407) was

collected from the – 200 m level of tunnels at the Gaofeng deposit in the Dachang ore field.

For Re–Os dating, molybdenite was separated by a steel needle and then handpicked under a binocular microscope. Re–Os isotope analyses were performed at the State Key Laboratory of Isotope Geochemistry, Guangzhou Institute of Geochemistry, Chinese Academy of Sciences. The analytical procedure for the determination of Re

concentrations and Os isotope ratios was described as follows: The  $^{185}\text{Re}$  spike, natural Os standard solutions and molybdenite samples (0.025–0.1 g) were weighed and digested with the concentrated  $\text{HNO}_3$  for 24 h at 240 °C in sealed Carius tubes. Os distilled as  $\text{OsO}_4$  from the supernatant was trapped using pure water and thus could be directly analyzed by ICP-MS. Re was determined by ICP-MS after separation and purification using anion exchange resin (AG1X8). Details of the analytical procedures are described in the references (Shirey and Walker 1995; Sun et al. 2010; Li et al. 2015).

The correction of Re isotopic ratios in the sample-spike mixtures was based on the factors calculated from the average ratios on the bracketed standards relative to the International Union of Pure and Applied Chemistry (IUPAC) ratios (Rosman and Taylor 1998). Mass bias correction for Os was ascertained on-line in each operational procedure. The mass bias factor for  $^{192}\text{Os}/^{187}\text{Os}$  was obtained by normalization to  $^{192}\text{Os}/^{188}\text{Os} = 3.08271$ . A range of 2% for the correction factors has been observed based on the results from the initial to final standard runs. Model ages were calculated using  $t = [\ln(1 + ^{187}\text{Os}/^{187}\text{Re})]/\lambda$ , where  $\lambda(^{187}\text{Re}) = 1.666 \times 10^{-11} \text{ a}^{-1}$  (Smoliar et al. 1996). Re–Os isochron age was calculated using ISOPLOT 3.0 (Ludwig 2003). Absolute uncertainties are given at  $2\sigma$  level (standard deviation). The molybdenite reference material of GBW04436 was repeatedly measured along with the samples. The Re–Os age of this reference material was  $140.4 \pm 2.3$  Ma ( $2 \text{ s}$ ,  $n = 4$ ). The result is consistent with certified values and the values previously reported by Du et al. (2004) and Li et al. (2010).

For in-situ Pb isotopes analyses, the samples were polished into thin sections and their surfaces were cleaned with ethanol, high-purity water and 2%  $\text{HNO}_3$  prior to analysis. In-situ Pb isotopes microanalyses of sulfides and feldspars were measured at the State Key Laboratory of Continental Dynamics, Northwest University, China. The analytical method has been previously described in detail by Chen et al. (2014), Yuan et al. (2015), and Bao et al. (2017).

It used LA-MC-ICP-MS, where the LA system was the 193 nm RESOLution M-50 (ASI, Australia), the MC-ICP-MS was the Nu Plasma II MC-ICP-MS by Nu Instruments (Nu Ins, UK), and the membrane desolvator system was Aridus II Desolvation Nebulizer System (Aridus II, Cetac, USA). Analytical signals could be deducted through the Time Resolved Analysis (TRA) mode. The integration time was approximately 0.2 s, the energy density was  $6 \text{ J/cm}^2$ , and the time of signal acquisition was 50 s. The laser frequency for galena was 3 Hz, with 13  $\mu\text{m}$  of spot size, for feldspar, molybdenite and pyrite was 6 Hz, with 100  $\mu\text{m}$  of spot size, respectively. Tl standard solution (NIST SRM 997) was introduced by membrane desolvator (50–100  $\mu\text{l/min}$ , PFA trace nebulizer) to calibrate Pb isotopes with the

fractionation factor calculated from  $^{203}\text{Tl}/^{205}\text{Tl}$  ratio (2.38890; Thirlwall 2002). Pb standard solution (NIST SRM 981) was used to monitor the accuracy and precision of instrumental analysis through desolvator. NIST SRM 610 reference glass was measured once for every five spots to be served as the external standard and quality control sample to monitor the reliability of Pb isotopic compositions. The results (isotope ratios) of NIST SRM 610 analysis were as follows:  $^{208}\text{Pb}/^{204}\text{Pb} = 36.968 \pm 0.007$ ,  $^{207}\text{Pb}/^{204}\text{Pb} = 15.512 \pm 0.003$ ,  $^{206}\text{Pb}/^{204}\text{Pb} = 17.051 \pm 0.003$ . The external accuracy of measurement of both  $^{206,207,208}\text{Pb}/^{204}\text{Pb}$  and  $^{207,208}\text{Pb}/^{206}\text{Pb}$  ratios was expected to be better than  $\pm 0.05\%$  (Chen et al. 2014). Considering this analytical method is not applicable for those minerals containing low Pb concentrations (< 10 ppm), in this study, feldspars and sulfides (e.g., molybdenite, pyrite and galena) with high Pb contents were selected for in-situ Pb isotopes microanalyses.

## 5 Results and discussions

### 5.1 Re–Os age of molybdenite

The Re–Os isotope data and model ages for six molybdenite samples from the Lamo Zn–Cu deposit are listed in Table 1. Re–Os isochron age is shown in Fig. 5.

The results show that Re and  $^{187}\text{Os}$  contents of the analyzed molybdenite samples varied from 1199.7 to 3005.0 and 1.1315 to 2.8226 ppb, respectively. Calculated Re–Os model ages of six samples were consistent, ranging from  $89.64 \pm 0.74$  to  $90.54 \pm 1.33$  Ma (Table 1). These samples yield a good Re–Os isochron age of  $90.0 \pm 1.1$  Ma with a MSWD of 0.72 (Fig. 5a), which is consistent with a weighted average model age of  $90.06 \pm 0.45$  Ma (Fig. 5b). This age is much younger than the reported garnet Sm–Nd isochron age of  $95 \pm 11$  Ma (Liang et al. 2011b) and quartz fluid inclusions Rb–Sr isochron age of  $99 \pm 6$  Ma (Li et al. 2008) for the Lamo deposit. Although there is no evidence that the molybdenite coexisted with the Zn–Cu sulfides at the Lamo deposit, they are hosted in the same skarn zones (Fig. 2b). Therefore, it is reasonable to infer that our molybdenite Re–Os age ( $90.0 \pm 1.1$  Ma) may be representative of the timing of Zn–Cu mineralization for the Lamo deposit.

Previous studies have reported the ages of several adjacent cassiterite-sulfide deposits in the Dachang ore field, using various isotope dating methods. Wang et al. (2004) obtained  $^{40}\text{Ar}-^{39}\text{Ar}$  plateau ages of  $94.5 \pm 0.3$  Ma for quartz and  $91.4 \pm 2.9$  Ma for sanidine from the No. 91 orebody in the Changpo-Tongkeng deposit, and of  $94.6 \pm 0.5$  Ma for quartz from the No. 100 orebody in the Gaofeng deposit. Cai et al. (2005, 2006b) reported the Rb–

**Table 1** Re and Os isotope data of molybdenite from the Lamo Zn–Cu deposit in the Dachang ore field

Sample	Weight (g)	Re $\pm 2\sigma$ (ppm)	$^{187}\text{Re} \pm 2\sigma$ (ppm)	$^{187}\text{Os} \pm 2\sigma$ (ppb)	Model age $\pm 2\sigma$ (Ma)
LM-601	0.2469	2.9778 $\pm$ 0.0352	1.8717 $\pm$ 0.0222	2.8226 $\pm$ 0.0263	90.45 $\pm$ 1.36
LM-603	0.3950	1.2827 $\pm$ 0.0125	0.8062 $\pm$ 0.0079	1.2097 $\pm$ 0.0160	90.00 $\pm$ 1.48
LM-604	0.3801	1.1997 $\pm$ 0.0124	0.7541 $\pm$ 0.0078	1.1315 $\pm$ 0.0087	90.00 $\pm$ 1.16
LM-605	0.2280	2.9748 $\pm$ 0.0339	1.8697 $\pm$ 0.0213	2.8225 $\pm$ 0.0163	90.54 $\pm$ 1.15
LM-606	0.1970	2.6748 $\pm$ 0.0240	1.6812 $\pm$ 0.0151	2.5378 $\pm$ 0.0297	90.54 $\pm$ 1.33
LM-607	0.1906	3.0050 $\pm$ 0.0170	1.8887 $\pm$ 0.0107	2.8226 $\pm$ 0.0168	89.64 $\pm$ 0.74

Model ages were calculated by:  $t = [\ln(1 + ^{187}\text{Os}/^{187}\text{Re})]/\lambda$ , where  $\lambda(^{187}\text{Re}) = 1.666 \times 10^{-11} \text{ a}^{-1}$  (Smoliar et al. 1996)

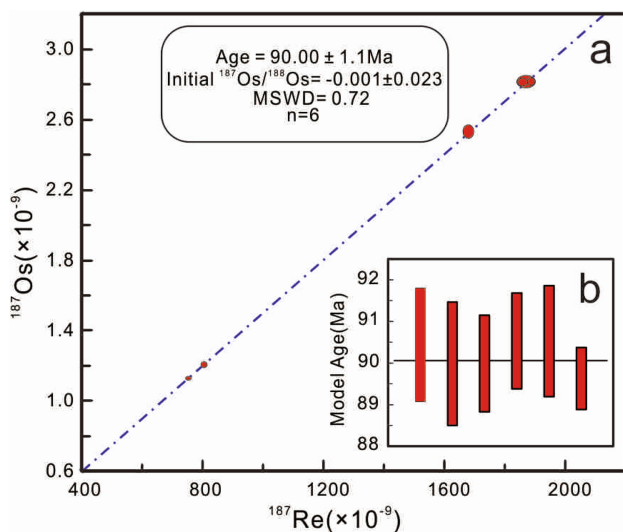


**Fig. 5** Re–Os isochron diagram (a) and weighted mean age diagram (b) of molybdenite from the Lamo Zn–Cu deposit

Sr isochron ages of  $93.4 \pm 7.9$  and  $94.1 \pm 2.7$  Ma for fluid inclusions of quartz from the No. 92 orebody of the Changpo-Tongkeng deposit and cassiterite-sulfide-quartz veins of the Kangma deposit, respectively. Recently, cassiterites from several cassiterite-sulfide deposits in the Dachang ore field have been dated using the LA-ICP-MS U–Pb method. Wang et al. (2015) and Guo et al. (2017) reported the cassiterite U–Pb ages of  $95.8 \pm 2.6$  and  $91$  to  $93$  Ma for the No. 92 orebody of the Changpo-Tongkeng deposit and the No. 100 orebody in the Gaofeng deposit, respectively. These ages, together with our molybdenite Re–Os age, overlap the ages of the granite and its porphyritic phase (91–97 Ma) in the Dachang ore field, suggesting that all of deposits in the Dachang were formed in a magmatic hydrothermal system related to the Longxianggai granite (Fu et al. 1991, 1993; Chen et al. 1993; Cai et al. 2005, 2007; Li et al. 2008).

## 5.2 In-situ Pb isotopes and source of metals

LA-MC-ICP-MS in situ Pb isotopic compositions of sulfides from the Lamo Zn–Cu deposit are listed in Table 2. Sulfide minerals analyzed include molybdenite, galena, and pyrite, whereas sphalerite and arsenopyrite cannot be measured because they have very low concentrations of Pb, which is the limit of the LA-MC-ICP-MS analysis.

A total of 19 spots for sulfides have been measured by LA-MC-ICP-MS. Seven spots on molybdenite have a range of  $^{206}\text{Pb}/^{204}\text{Pb}$  ratios from 18.532 to 18.565,  $^{207}\text{Pb}/^{204}\text{Pb}$  from 15.715 to 15.746, and  $^{208}\text{Pb}/^{204}\text{Pb}$  from 38.947 to 39.033 (Table 2; Fig. 6a, b). One spot on molybdenite (LM602-MO-4) has relatively lower Pb isotopic compositions ( $^{206}\text{Pb}/^{204}\text{Pb} = 18.475$ ,  $^{207}\text{Pb}/^{204}\text{Pb} = 15.661$ ,  $^{208}\text{Pb}/^{204}\text{Pb} = 38.818$ ). This difference may be attributed to its lower concentration of Pb that is close to the limit of LA-MC-ICP-MS analysis. Model ages of molybdenite (216–234 Ma) are incompatible (too old) as compared with their Re–Os age of 90 Ma obtained from this study. Galena has a narrow range of  $^{206}\text{Pb}/^{204}\text{Pb}$  ratios from 18.515 to 18.517,  $^{207}\text{Pb}/^{204}\text{Pb}$  from 15.701 to 15.705, and  $^{208}\text{Pb}/^{204}\text{Pb}$  from 38.945 to 38.993. The  $^{206}\text{Pb}/^{204}\text{Pb}$  ratios of pyrite vary from 18.489 to 18.523,  $^{207}\text{Pb}/^{204}\text{Pb}$  from 15.693 to 15.711, and  $^{208}\text{Pb}/^{204}\text{Pb}$  from 38.917 to 38.991. All of Pb isotope data plot along a steep slope that lies mostly above the average crustal Pb model curve of Zartman and Deo (1981) (Fig. 6a) and overlaps the range of previous sulfides and sulfosalts conventionally determined by bulk analyses (Fig. 6c, d).

To compare the Pb isotopic compositions for sulfides, less altered feldspars in the granite and its porphyritic phase (Fig. 4i–l) from the Dachang ore field are measured by LA-MC-ICP-MS, which are listed in Table 2. Eleven spots on different feldspar grains in the granite have a larger range of  $^{206}\text{Pb}/^{204}\text{Pb}$  ratios from 18.417 to 18.594,  $^{207}\text{Pb}/^{204}\text{Pb}$  from 15.641 to 15.728, and  $^{208}\text{Pb}/^{204}\text{Pb}$  from 38.791 to 39.073 (Table 2). The  $^{206}\text{Pb}/^{204}\text{Pb}$  ratios of feldspars in the granite porphyry dikes vary from 18.467 to 18.546,  $^{207}\text{Pb}/^{204}\text{Pb}$  from 15.672 to 15.743, and  $^{208}\text{Pb}/^{204}\text{Pb}$  from 38.895 to 39.065. These data also plot along a steep

**Table 2** In-situ Pb isotope data of sulfides from the Lamo Zn–Cu deposit and feldspars in the granites from the Dachang ore field

Sample no.	Mineral	$^{206}\text{Pb}/^{204}\text{Pb}$	$1\sigma$	$^{207}\text{Pb}/^{204}\text{Pb}$	$1\sigma$	$^{208}\text{Pb}/^{204}\text{Pb}$	$1\sigma$	$\mu$ value	T (Ma)
<i>Sulfides from 680 m level at the Lamo deposit</i>									
LM602-MO-1	Molybdenite	18.535	0.012	15.720	0.011	38.961	0.026	9.69	225
LM602-MO-2	Molybdenite	18.532	0.016	15.718	0.014	38.947	0.035	9.68	225
LM602-MO-3	Molybdenite	18.535	0.012	15.724	0.011	38.989	0.027	9.69	229
LM602-MO-4	Molybdenite	18.475	0.035	15.661	0.030	38.818	0.073	9.58	196
LM602-MO-5	Molybdenite	18.537	0.027	15.715	0.023	38.959	0.057	9.68	218
LM602-MO-6	Molybdenite	18.547	0.031	15.719	0.027	38.983	0.066	9.68	216
LM602-MO-7	Molybdenite	18.542	0.067	15.726	0.057	39.009	0.142	9.70	228
LM602-MO-8	Molybdenite	18.565	0.045	15.746	0.037	39.033	0.094	9.73	234
LM613-GN-1	Galena	18.515	0.002	15.704	0.003	38.945	0.008	9.66	219
LM613-GN-2	Galena	18.515	0.002	15.705	0.002	38.950	0.007	9.66	220
LM613-GN-3	Galena	18.515	0.002	15.701	0.002	38.984	0.007	9.65	216
LM613-GN-4	Galena	18.517	0.003	15.704	0.003	38.993	0.009	9.66	219
LM613-PY-1	Pyrite	18.489	0.035	15.695	0.030	38.930	0.075	9.64	227
LM613-PY-2	Pyrite	18.513	0.003	15.698	0.003	38.917	0.008	9.65	214
LM613-PY-3	Pyrite	18.523	0.007	15.711	0.006	38.958	0.015	9.67	222
LM613-PY-4	Pyrite	18.510	0.009	15.701	0.008	38.968	0.019	9.65	220
LM613-PY-5	Pyrite	18.513	0.005	15.702	0.004	38.971	0.011	9.65	219
LM613-PY-6	Pyrite	18.508	0.002	15.693	0.002	38.975	0.007	9.64	212
LM613-PY-7	Pyrite	18.517	0.002	15.704	0.002	38.991	0.007	9.66	218
<i>Feldspars of biotite granite from 590 m and 530 m levels at the Lamo deposit</i>									
LM590-FSP-1	Feldspar	18.459	0.030	15.712	0.024	38.889	0.064	9.68	269
LM590-FSP-2	Feldspar	18.474	0.017	15.694	0.015	38.947	0.037	9.64	237
LM590-FSP-3	Feldspar	18.536	0.023	15.718	0.019	39.025	0.049	9.68	222
LM590-FSP-4	Feldspar	18.547	0.019	15.709	0.016	39.004	0.041	9.66	203
LM590-FSP-5	Feldspar	18.568	0.029	15.722	0.025	39.004	0.061	9.69	203
LM590-FSP-6	Feldspar	18.594	0.031	15.728	0.026	39.073	0.063	9.70	193
LM530-FSP-1	Feldspar	18.417	0.045	15.641	0.039	38.791	0.099	9.54	213
LM530-FSP-2	Feldspar	18.474	0.024	15.684	0.021	38.942	0.052	9.62	225
LM530-FSP-3	Feldspar	18.505	0.045	15.715	0.038	39.060	0.095	9.68	240
LM530-FSP-4	Feldspar	18.436	0.044	15.661	0.037	38.959	0.092	9.58	223
LM530-FSP-5	Feldspar	18.495	0.028	15.713	0.024	39.008	0.059	9.68	245
<i>Feldspars of granite porphyry from – 200 m level at the Gaofeng deposit</i>									
GF407-FSP-1	Feldspar	18.467	0.012	15.685	0.011	38.900	0.028	9.62	231
GF407-FSP-2	Feldspar	18.485	0.014	15.702	0.012	38.924	0.031	9.66	238
GF407-FSP-3	Feldspar	18.502	0.019	15.702	0.016	38.952	0.041	9.66	227
GF407-FSP-4	Feldspar	18.546	0.026	15.743	0.022	39.065	0.055	9.73	244
GF407-FSP-5	Feldspar	18.468	0.019	15.672	0.017	38.895	0.041	9.60	214

slope that lies mostly above the average crustal Pb model curve (Fig. 6c, d), which are similar to the in-situ Pb isotopes of sulfides. However, the in-situ Pb isotopes of feldspars are much different than those of the reported whole-rock granites that were conventionally determined by bulk analyses (Fig. 6c, d). The reasons are unknown, possibly U loss caused by weathering and hydrothermal alteration of granites (Tosdal et al. 1999). The overlapping

of in-situ Pb isotopic compositions between sulfides and feldspars from the Dachang ore field suggests that the metals were mainly sourced from Cretaceous granitic magma.

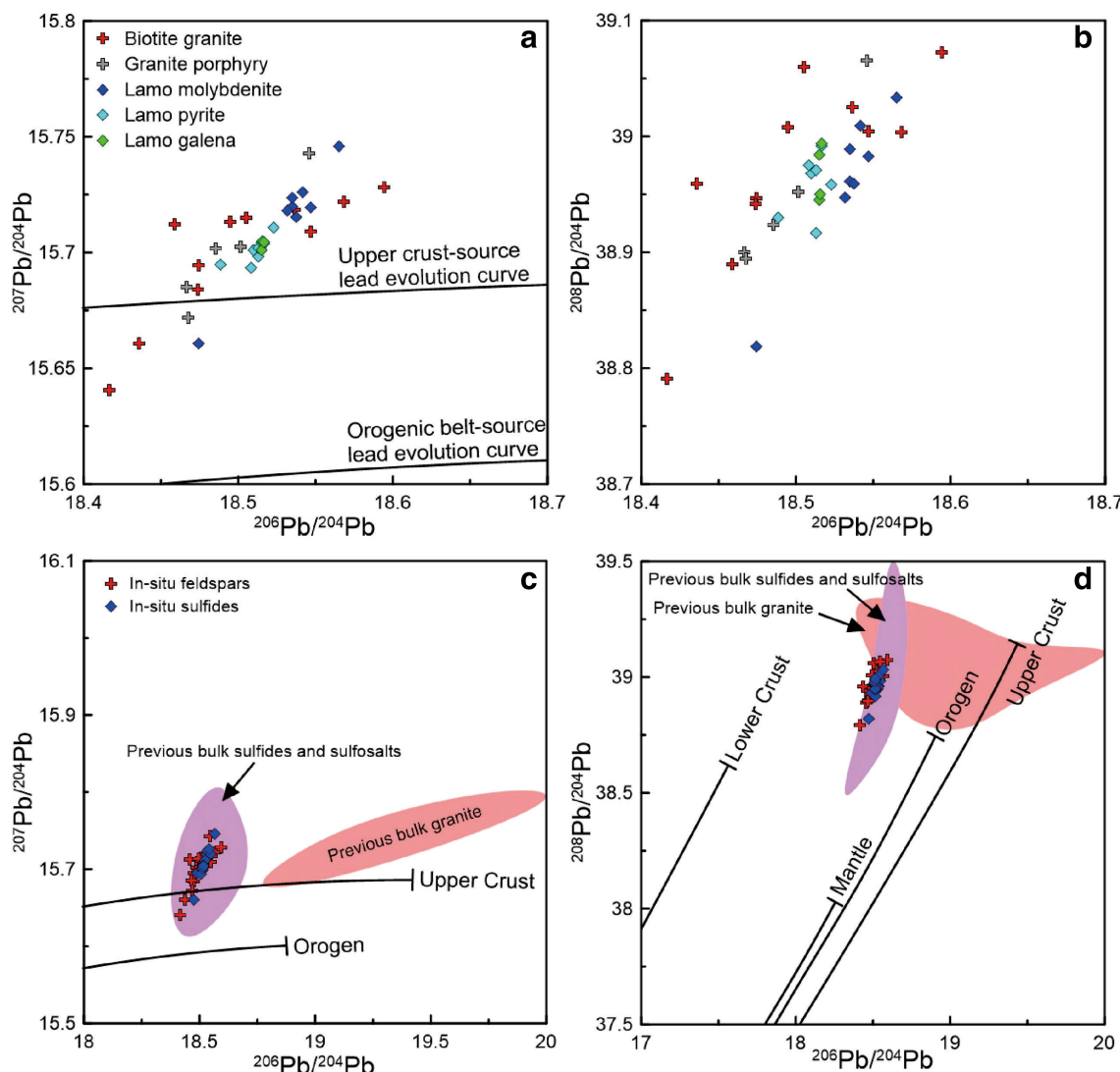


**Fig. 6** In-situ Pb isotope compositions of sulfides from the Lamo Zn–Cu deposit and feldspars in the granite and granitic porphyry dike from the Dachang ore field. **a**  $^{207}\text{Pb}/^{204}\text{Pb}$  versus  $^{206}\text{Pb}/^{204}\text{Pb}$ ; **b**  $^{208}\text{Pb}/^{204}\text{Pb}$  versus  $^{206}\text{Pb}/^{204}\text{Pb}$ . **c, d** Comparison of in-situ and bulk Pb isotopes data from the Dachang ore field. The bulk Pb isotopes data are from Ding et al. (1988), Chen et al. (1993), Han et al. (1997), Gao (1999), Qin et al. (2002), Zhao et al. (2007), Liang et al. (2008), and Cheng and Peng (2014). Lead evolution curves are from Zartman and Doe (1981)

## 6 Conclusions

This study presents a new molybdenite Re–Os age and in-situ Pb isotopes of sulfides from the Lamo Zn–Cu deposit in the Dachang ore field. Molybdenite Re–Os dating yields a reliable and accurate isochron age of  $90.0 \pm 1.1$  Ma. This new age is close to the ages of cassiterite (91–96 Ma) and the granite and its porphyritic phase (91–97 Ma) in the Dachang ore field, suggesting that all of deposits in the Dachang were formed in the Cretaceous granite-related magmatic hydrothermal system.

In-situ Pb isotopes of sulfides from the Lamo deposit have similar ranges of Pb isotopic compositions of the feldspars in the biotite granite and granitic porphyry dikes in the district, suggesting that the metals were mainly

sourced from a granitic magma that was derived from melting of the upper crust.

**Acknowledgements** We gratefully acknowledge the Mining Company of Jilang Indium Industry for access to samples. This work is supported by the National Science Foundation of China (Grants Nos. 41672080, 41772079, 41272113) and Outstanding Talent Foundation of the Institute of Geochemistry, Chinese Academy of Sciences.

### Compliance with ethical standards

**Conflict of interest** There is no conflict of interest.

## References

- Bao ZA, Chen L, Zong CL, Yuan HL, Chen KY, Dai MN (2017) Development of pressed sulfide powder tablets for *in-situ* sulfur and lead isotope measurement using LA-MC-ICP-MS. *Int J Mass Spectrom* 421:255–262
- Cai HY, Zhang GL (1983) On submarine volcanism hot spring (exhalative) mineralization of the Dachang tin polymetallic deposit in Guangxi. *Bull Inst Miner Resour Geol* 1(4):13–21 (in Chinese)
- Cai MH, Liang T, Wu DC, Huang HM (2004) Structure characteristics and mineralization controls of the Nandan-Hechi metallogenetic belt in Guangxi Province. *Geol Prospect* 40:5–10 (in Chinese with English abstract)
- Cai MH, Liang T, Wu DC (2005) Geological characteristics and ore-forming time of the Kangma deposit in the Dachang tin-polymetallic ore field, Guangxi. *Acta Geol Sin* 79:262–268 (in Chinese with English abstract)
- Cai MH, He LQ, Liu GQ, Wu DC, Huang HM (2006a) SHRIMP zircon U–Pb dating of the intrusive rocks in the Dachang tin-polymetallic ore field, Guangxi and their geological significance. *Geol Rev* 52:409–414 (in Chinese with English abstract)
- Cai MH, Liang T, Wei KL, Huang HM, Liu GQ (2006b) Rb–Sr dating of the No. 92 orebody of the Tongkeng-Changpo deposit in the Dachang tin polymetallic ore field, Guangxi, and its significance. *Geol Miner Resour South China* 2:35–42 (in Chinese with English abstract)
- Cai MH, Mao JW, Liang T, Pirajno F, Huang HL (2007) The origin of the Tongkeng-Changpo tin deposit, Dachang metal district, Guangxi, China: clues from fluid inclusions and He isotope systematics. *Miner Depos* 24:613–626
- Chen YC, Huang MZ, Xu J, Ai YD, Li XM, Tang SH, Meng LK (1985) Geological features and metallogenetic series of the Dachang cassiterite-sulfide-polymetallic belt. *Acta Geol Sin* 3:228–240 (in Chinese with English abstract)
- Chen YC, Huang MZ, Xu J, Hu YZ, Tang SH, Li YQ, Meng LK (1993) Tin deposits of Dachang. Geological Publishing House, Beijing (in Chinese with English abstract)
- Chen KY, Yuan HL, Bao ZA, Zong CL, Dai MN (2014) Precise and accurate *in-situ* determination of lead isotope ratios in NIST, USGS, MPI-DING and CGSG glass reference materials using femtosecond laser ablation MC-ICP-MS. *Geostand Geoanal Res* 38:5–21
- Cheng YS, Peng C (2014) Ore-forming material of Dachang tin deposit in Guangxi, China: lead isotope evidence. *Trans Nonferrous Met Soc China* 24:3652–3659
- Ding TP, Peng ZC, Ni H, Li YH (1988) Stable isotope studies on several typical mineral deposits in the Nanling region. Beijing Science and Technology Publishing House, Beijing (in Chinese with English abstract)
- Du AD, Wu SQ, Sun DZ, Wang SX, Qu WJ, Markey R, Stein HJ, Morgan JW, Malinovskiy D (2004) Preparation and certification of Re–Os dating reference materials: molybdenite HLP and JDC. *Geostand Geoanal Res* 28:41–52
- Fan DL, Zhang T, Ye J, Pašava J, Kribek B, Dobes P, Varrin I, Zak K (2004) Geochemistry and origin of tin-polymetallic sulfide deposits hosted by the Devonian black shale series near Dachang, Guangxi, China. *Ore Geol Rev* 24:103–120
- Fu M, Changkakoti A, Krouse HR, Gray J, Kwak TAP (1991) An oxygen, hydrogen, sulfur, and carbon isotope study of carbonate-replacement (skarn) tin deposits of the Dachang tin field, China. *Econ Geol* 86:1683–1703
- Fu M, Kwak TAP, Mernagh TP (1993) Fluid inclusion studies of zoning in the Dachang tin-polymetallic ore field, People's Republic of China. *Econ Geol* 88:283–300
- Gao JY (1999) Pb isotopic evolution and its significance in ore genesis in the Dachang tin-polymetallic ore deposits. *Geol Geochem* 27(2):38–43 (in Chinese with English abstract)
- Guo J, Sun WD, Zhang RQ, Hu YB (2017) Cassiterite U–Pb geochronology and trace element fingerprints of the Gaofeng tin deposit, Dachang district, South China. SEG 2017 Abstract, Beijing, China, p 170
- Han F, Hutchinson RW (1989a) Evidence for exhalative origin for rocks and ores of the Dachang tin polymetallic field: the ore-bearing formation and hydrothermal exhalative sedimentary rocks. *Miner Depos* 8:25–40 (in Chinese with English abstract)
- Han F, Hutchinson RW (1989b) Evidence for hydrothermal exhalative sedimentary origin of the Dachang tin-polymetallic deposits-geochemistry of rare earth elements and trace elements of the host rocks. *Miner Depos* 8(3):33 (in Chinese with English abstract)
- Han F, Zhao RS, Shen JZ, Hutchinson RW, Jiang SY (1997) Geology and origin of ores in the Dachang polymetallic tin ore field. Geological Publishing House, Beijing (in Chinese with English abstract)
- Huang WH, Fan SK, Chen CW, Bi ZM (2012) Application of metallogenetic regularity to study of skarn zinc-copper deposits in Dachang ore field: a case study of Heishiguogou-Dashujiao and Yangjiaojian skarn zinc-copper deposits. *Miner Depos* 31:535–544 (in Chinese with English abstract)
- Jiang SY, Han F, Shen JZ, Palmer MR (1999) Chemical and Rb–Sr, Sm–Nd isotopic systematics of tourmaline from the Dachang Sn-polymetallic ore deposit, Guangxi, China. *Chem Geol* 157:49–67
- Kwak TAP (1987) W-Sn skarn deposits and related metamorphic skarns and granitoids. Elsevier 24:1–451
- Li HQ, Wang DH, Mei YP, Liang T, Cheng ZY, Guo CL, Ying LJ (2008) Lithogenesis and mineralization chronology study on the Lamo zinc–copper polymetallic ore deposit in Dachang orefield, Guangxi. *Acta Geol Sin* 82:912–919 (in Chinese with English abstract)
- Li J, Zhong LF, Tu XL, Liang XR, Xu JF (2010) Determination of rhodium content in molybdenite by ICP-MS after separation of the major matrix by solvent extraction with N-benzoyl-N-phenylhydroxalamine. *Talanta* 81:954–958. <https://doi.org/10.1016/j.talanta.2010.01.043>
- Li J, Zhao PP, Liu JG, Wang XC, Yang Y, Wang GQ, Xu JF (2015) Reassessment of hydrofluoric acid desilicification in the Carius tube digestion technique for Re–Os isotopic determination in geological samples. *Geostand Geoanal Res* 39(1):17–30
- Liang T, Chen YC, Wang DH, Cai MH (2008) The geological and geochemical characteristics of Dachang tin-polymetallic deposit, Guangxi. Geological Publishing House, Beijing (in Chinese with English abstract)
- Liang T, Wang DH, Hou KJ, Li HQ, Huang HM, Cai MH, Wang DM (2011a) LA-MC-ICP-MS zircon U–Pb dating of Longxianggai pluton in Dachang of Guangxi and its geological significance. *Acta Petrol Sin* 27:1624–1636 (in Chinese with English abstract)
- Liang T, Wang DH, Li HQ, Huang HM, Wang DM, Ping Yu, Cai MH (2011b) REE geochemistry and Sm–Nd isotope age of garnet from the Dachang, Guangxi. *J Northwest Univ* 41(4):676–681 (in Chinese with English abstract)
- Luck JM, Allègre CJ (1982) The study of molybdenites through the  $^{187}\text{Re}$ – $^{187}\text{Os}$  chronometer. *Earth Planet Sci Lett* 61:291–296
- Ludwig KR (2003) ISOPLOT 3.00: a geochronological toolkit for Microsoft Excel. Berkeley Geochronology Center, Berkeley
- Pašava J, Kříbek B, Dobeš P, Vavřín I, Žák K, Fan DL, Zhang T, Boiron MC (2003) Tin-polymetallic sulfide deposits in the eastern part of the Dachang tin field (South China) and the role of black shales in their origin. *Miner Depos* 38:39–66

- Qin DX, Hong T, Tian YL, Chen JW (2002b) Ore geology and technical economy of No 92 orebody of the Dachang tin deposit, Guangxi. Geological Publishing House, Beijing (**in Chinese with English abstract**)
- Rosman KJR, Taylor PDP (1998) Isotopic compositions of the elements 1997. Pure Appl Chem 70:217–238
- Selby D, Creaser RA (2001) Re–Os geochronology and systematics in molybdenite from the Endako porphyry molybdenum deposit, British Columbia, Canada. Econ Geol 96:197–204
- Shirey S, Walker R (1995) Carius tube digestion for low-blank Rhodium–Osmium analysis. Anal Chem 67:2136–2141
- Smoliar MI, Walker RJ, Morgan JW (1996) Re–Os ages of group IIA, IIIA, IVA, and IVB iron meteorites. Science 271:1099–1102
- Stein HJ, Markey RJ, Morgan JW, Hannah JL, Scherstén A (2001) The remarkable Re–Os chronometer in molybdenite: how and why it works. Terra Nova 13:479–486
- Sun YL, Xu P, Li J, He K, Chu ZY, Wang Y (2010) A practical method for determination of molybdenite Re–Os age by inductively coupled plasma-mass spectrometry combined with Carius tube-HNO<sub>3</sub> digestion. Anal Methods 2:575–581
- Thirlwall MF (2002) Multicollector ICP-MS analysis of Pb isotopes using a <sup>207</sup>Pb–<sup>204</sup>Pb double spike demonstrates up to 400 ppm/amu systematic errors in Th-normalization. Chemical Geology 184(3–4):255–279. [https://doi.org/10.1016/S0009-2541\(01\)00365-5](https://doi.org/10.1016/S0009-2541(01)00365-5)
- Tosdal RM, Wooden JL, Bouse R (1999) Pb isotopes, ore deposits, and metallogenic terranes. In: Lambert DD, Ruiz J (eds) Application of radiogenic isotopes to ore deposit research and exploration. Reviews Economic Geology 12:1–28
- Wang DH, Chen YC, Chen W, Sang HQ, Li HQ, Lu YF, Chen KL, Lin ZM (2004) Dating the Dachang giant tin-polymetallic deposit in Nandan, Guangxi. Acta Geol Sin 78:132–138 (**in Chinese with English abstract**)
- Wang XY, Huang HW, Chen NS, Huang XQ, Wu XK, Hao S, Li HM (2015) *In-situ* LA-MC-ICPMS U–Pb geochronology of cassiterite from Changpo-Tongkeng tin-polymetallic deposits, Dachang ore field, Guangxi. Geol Rev 61:892–900 (**in Chinese with English abstract**)
- Xu M, Cai MH, Peng ZA, Zhang SQ, Chen Y, Wang XB (2011) Characteristics of structures and controls on mineralization of Tongkeng tin-polymetallic deposit in Guangxi. Geotecton Metallog 35:587–595 (**in Chinese with English abstract**)
- Ye XS, Pan QY (1994) Discovery history of Dachang tin-polymetallic orefield, Nandan County, Guangxi. Guangxi Geol 7(1):85–94 (**in Chinese with English abstract**)
- Yuan HL, Yin C, Liu X, Chen KY, Bao ZA, Zong CL, Dai MN, Lai SC, Wang R, Jiang SY (2015) High precision *in-situ* Pb isotopic analysis of sulfide minerals by femtosecond laser ablation multicollector inductively coupled plasma mass spectrometry. Sci China Earth Sci 58:1713–1721
- Zartman RE, Doe BR (1981) Plumbotectonics—the model. Tectono-physics 75:135–142
- Zhao KD, Jiang SY, Xiao HQ, Ni P (2002) Origin of ore-forming fluids of the Dachang Sn-polymetallic ore deposit: evidence from helium isotopes. Chin Sci Bull 47(12):1041–1045
- Zhao KD, Jiang SY, Ni P, Ling HF, Jiang YH (2007) Sulfur, lead and helium isotopic compositions of sulfide minerals from the Dachang Sn-polymetallic ore district in South China: implication for ore genesis. Miner Pet 89:251–273